
**SURFACE,
ELECTRON AND ION EMISSION**

Surface Morphology and Optical and Magnetic Properties of Polyelectrolyte/Magnetite Nanoparticles Nanofilms

D. A. Gorin^a, A. M. Yashchenok^a, Yu. A. Koksharov^b, A. A. Neveshkin^a,
A. A. Serdobintsev^a, D. O. Grigoriev^c, and G. B. Khomutov^b

^a Chernyshevsky State University, Saratov, 410012 Russia

e-mail: GorinDA@mail.ru, GorinDA@sgu.ru

^b Moscow State University, Moscow, 119899 Russia

^c Max Planck Institute of Colloids and Interfaces, Potsdam, D14424 Germany

Received September 18, 2008

Abstract—Polyelectrolyte/iron oxide nanoparticles composite nanocoatings are fabricated by polyionic assembly. They are characterized by atomic force microscopy, electron magnetic resonance, ellipsometry, and secondary-ion mass spectrometry. The results obtained indicate that the number of magnetite nanoparticle layers in a film is related to its refractive index, thickness, and surface roughness. The electron magnetic resonance signal intensity is found to nonlinearly depend on the number of magnetic nanoparticle layers in a film.

PACS numbers: 68.35.B-, 68.35.-d, 75.70.-i, 78.66.-w

DOI: 10.1134/S1063784209110206

INTRODUCTION

The search for novel materials for the designing and creation of electronic and optoelectronic nanodevices and functional circuits of various purposes is a challenging problem. Today, nanotechnologies present new approaches to developing artificial nanostructured media and the most promising approach consists in the self-organization of molecules and nanocomposites. Methods based on this approach include the Langmuir–Blodgett method [1, 2], centrifugation [3], sputtering [4, 5], and polyionic assembly [6].

Among these methods, polyionic assembly is the most promising method; it is based on the sequential adsorption of polyionic molecules and/or charged colloidal particles [7, 8]. Using polyionic self-assembly, one can grow both polyelectrolyte multilayer structures and composite coatings with embedded nanocomposites of various natures [7, 9–11]. Such 2D nanostructures represent a multiphase system consisting of a polymer matrix and such elements as inorganic nanoparticles of various compositions and shapes. The properties of these nanoobjects can differ substantially from those of the corresponding bulk materials [12, 13].

In the case of semiconductor nanoparticles, the so-called quantum size effect is known to take place [13]. It is also known that the magnetization and magnetic anisotropy of magnetic nanoparticles can be several times higher than those of the corresponding bulk materials. Moreover, nanoparticles were used as the basis for structures that exhibit a giant magnetoresistance, the magnetocaloric effect, and so on [14, 15].

Since magnetic iron oxides (magnetite, maghemite) are semiconductors, it is important to perform studies in the field of the creation and investigation of the properties of organized nanostructures based on magnetic nanophase iron oxides.

The authors of [7] showed that, for nanocomposite coatings based on polydimethylallyl ammonium chloride and containing magnetite nanoparticles, the absorption spectrum of a nanocomposite film in the near infrared (IR) region has a spectral window near 1500 nm. This specific feature of nanocomposite films opens up fresh opportunities for using them as coatings with a given reflectance for creating interference mirrors when designing semiconductor IR lasers. Moreover, nanocomposite coatings containing magnetic nanoparticles are promising materials for permanent magnets [15], storage medium, functional elements in magnetic sensors [12], and radio-absorbing coatings [16, 17].

The properties of nanocomposite materials depend on the fraction of inorganic particles in a polymer matrix. Depending on the filling of a dielectric matrix with inorganic nanoparticles, the properties of such nanocomposites can vary over wide limits and exhibit quantum size effects [13]. In addition, the properties of nanocomposites are likely to depend on the choice of a polymer matrix and the shape, size, and chemical composition of nanoparticles. In [18, 19], we showed that the thickness, refractive index, and surface roughness of a nanocomposite coating increase with the number of magnetite nanoparticle layers.

A practical application of such systems implies the investigation of their optical and magnetic properties.

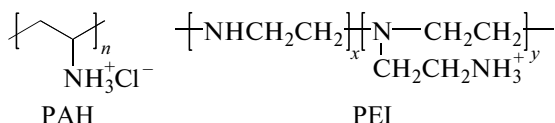


Fig. 1. Structural formulas of the monomeric units of the polyionic molecules.

Moreover, to study the dependence of the physical properties of nanocomposite coatings on the volume fraction of nanoparticles, one should use methods that can determine and control the chemical composition of nanocoatings.

Therefore, the purpose of this work was to study the physical properties of nanocomposite coatings based on polyallylaminehydrochloride/iron oxide nanoparticles as a function of the volume fraction of nanoparticles in them. For examination, we applied electron magnetic resonance, secondary-ion mass spectrometry, ellipsometry, and atomic force microscopy.

EXPERIMENTAL

Materials

To prepare nanocomposite coatings, we used 0.5M NaCl aqueous solutions of polyallylaminehydrochloride (PAH, $MW \sim 70\,000$) and polyethyleneimine (PEI, $MW \sim 600\,000$ – $1\,000\,000$) molecules (Sigma-Aldrich Co.) at a concentration of 2 mg/ml (Fig. 1) [20]. We also used aqueous suspensions of iron oxide Fe_3O_4 nanoparticles (Berlin Heart) at a concentration of 3.2 mg/ml. The nanoparticles were stabilized by citric acid (the Z potential of nanoparticles in an aqueous solution with $\text{pH} = 6.9 \pm 0.2$ was -47.7 mV), and the average nanoparticle size was ≈ 10 nm [21].

As substrates, we employed chemically cleaned single-crystal (111) silicon wafers. They were boiled in carbon tetrachloride for 15 min, etched in hydrofluoric acid, and rinsed with distilled water. As a result, the substrate surface had a negative charge in a water phase at $\text{pH} = 5$ – 7 [22].

To increase the efficiency of the polyelectrolyte film formation and to decrease the film roughness, we used polyethyleneimine to create the first polymer layer [23, 24]. PAH and Fe_3O_4 nanoparticles were alternatively deposited onto silicon wafers in a computer-assisted Poliion-1M device (Saratov, Russia) [18]. The nanocomposite films deposited onto single-crystal silicon wafers had the following composition: PEI/ $(\text{Fe}_3\text{O}_4/\text{PAH})_N$, where $N = 6, 11, 16$.

Experimental Techniques

Atomic force microscopy (AFM). AFM images of nanocomposite films were taken with an INTEGRA SPECTRA (NT-MDT, Russia) microscope in the tapping mode at room temperature (we used cantile-

vers with a resonance frequency of 302–354 kHz and a bending stiffness of 25–42 N/m). To determine the film thickness, we mechanically removed a local area in a nanocomposite coating and measured the difference between the heights of the uncoated and coated substrate.

The AFM images of nanocomposite films were processed with the Gwyddion 2.9 visualization and analysis software package in order to determine the film roughness and thickness. Roughness is known to characterize the uniformity of the film in the direction normal to the substrate/film interface. The average nanocomposite film thickness was determined from at least five height profiles measured on one sample.

Ellipsometry. We used ellipsometry to measure the optical parameters and thickness of nanocomposite coatings on single-crystal silicon wafers. Polarization angles Ψ and Δ were measured with an LEF-3M null ellipsometer (wavelength 632.8 nm) in air at angles of incidence of 60° and 70° . Refractive index n and film thickness δ were determined from experimentally measured polarization angles Ψ and Δ using the single-layer isotropic nonabsorbing film–absorbing isotropic substrate model [18, 25].

Secondary-ion mass spectrometry (SIMS). SIMS studies of nanocomposite films were performed on a device based on an MI-1305 mass spectrometer [26]. An ion beam consisting of positively charged 4- to 8-keV oxygen ions bombarded a sample at an angle of 60° to the normal. The focusing system of the device provided an ion beam 1 mm in diameter. The primary-beam current was 1–10 μA ; as a result a substrate was insignificantly heated. The mass numbers to be detected ranged from 1 to 240.

Electron magnetic resonance (EMR). EMR studies of polyelectrolyte/magnetite nanoparticles films were carried out with a Varian E-4 EPR X (9.2 GHz) spectrometer at room temperature on rectangular 4 × 10-mm samples.

RESULTS AND DISCUSSION

Figure 2 shows AFM images of the surfaces of nanocomposite films. Arithmetical mean roughness R_a of the films was 10 ± 1 , 15 ± 1 , and 18 ± 2 nm for $N = 6, 11$, and 16 (where N is the number of magnetite nanoparticle layers), respectively. These roughnesses are seen to be comparable with or larger than the average nanoparticle size. For a nanocomposite film with $N = 16$, the roughness is more than twice as large as the nanoparticle size. The increase in the roughness indicates the formation of clusters or aggregates from nanoparticles, which also promotes a further increase in the film roughness during the further growth.

Table 1 gives the film thickness determined by AFM and ellipsometry without regard for the absorption in nanocomposite coatings.

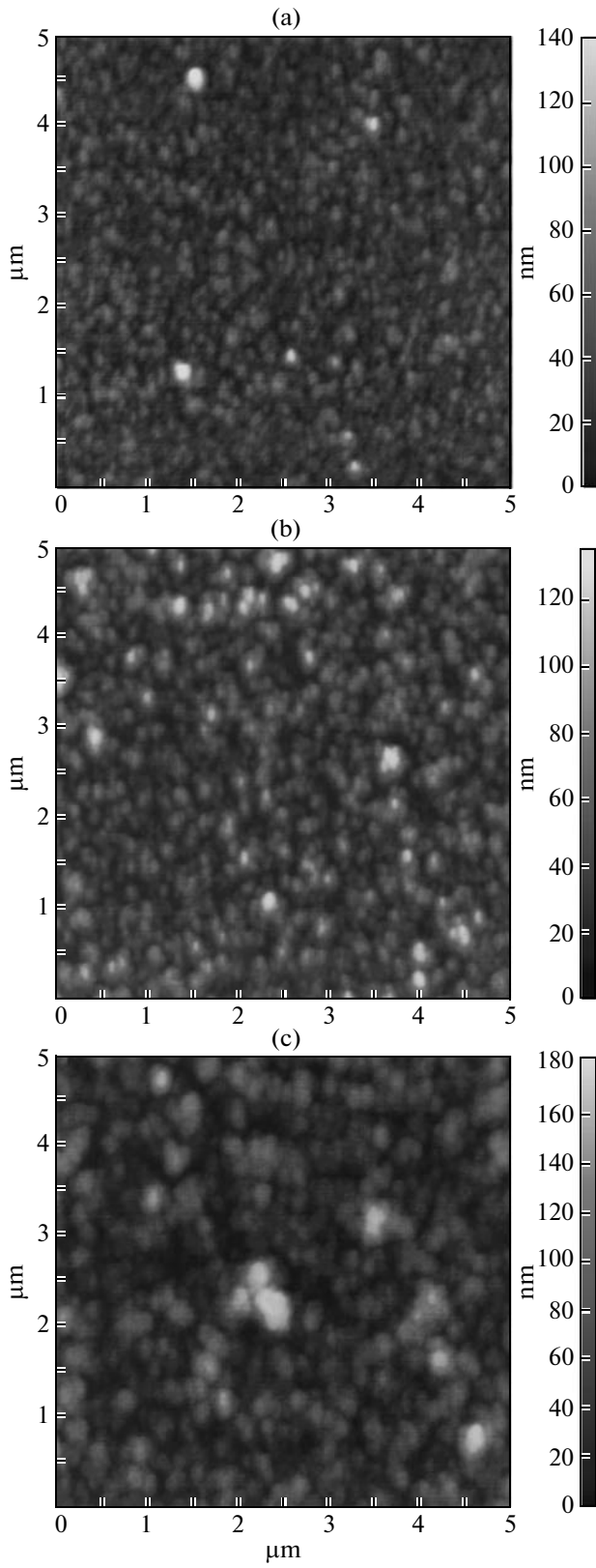


Fig. 2. AFM images of nanocomposite films: (a) $\text{PEI}/(\text{Fe}_3\text{O}_4/\text{PAH})_6$, (b) $\text{PEI}/(\text{Fe}_3\text{O}_4/\text{PAH})_{11}$, and (c) $\text{PEI}/(\text{Fe}_3\text{O}_4/\text{PAH})_{16}$.

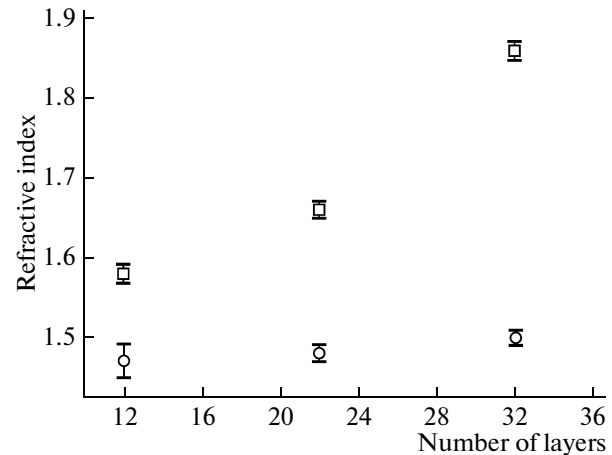


Fig. 3. Refractive index of a nanofilm vs. the number of adsorbed layers: (circles) $\text{PEI}/(\text{PAH}/\text{PSS})$ and (squares) $\text{PEI}/(\text{Fe}_3\text{O}_4/\text{PAH})$.

Figure 3 shows the refractive index of the nanocomposite films as a function of the number of adsorbed layers and the refractive indices of polyelectrolyte coatings free of magnetite nanoparticles. The average refractive index ($n_a = 1.48$) and the average layer thickness ($\delta = 2.1 \pm 0.1 \text{ nm}$) of the $\text{PEI}/(\text{PAH}/\text{PSS})$ films and the dependence of the film thickness on the number of adsorbed layers agree with the results in [27, 28]. The thickness and refractive index of the nanocomposite films change as the fraction of magnetite nanoparticles in a polyelectrolyte film increases. The use of iron oxide nanoparticles for creating nanocomposite coatings leads to an increase in the refractive index of the film and its thickness at the same number of layers.

We estimated the volume fraction f of iron oxide nanoparticles in nanocomposite films using an effective dielectric medium model. In general form, we can calculate effective permittivity ϵ_{eff} of a host medium (with permittivity ϵ_h) containing two types of spherical inclusions with permittivities ϵ_a and ϵ_b using the expression [29]

$$\frac{\epsilon_{\text{eff}} - \epsilon_h}{\epsilon_{\text{eff}} + 2\epsilon_h} = f_a \frac{\epsilon_a - \epsilon_h}{\epsilon_a + 2\epsilon_h} + f_b \frac{\epsilon_b - \epsilon_h}{\epsilon_b + 2\epsilon_h} + \dots, \quad (1)$$

where f_a and f_b are the volume fractions of the components with permittivities ϵ_a and ϵ_b , respectively. For our films, we employed the following two approximations [29]:

Maxwell–Garnett (MG) approximation

$$f_a = \left(\frac{\epsilon_{\text{eff}} - \epsilon_b}{\epsilon_{\text{eff}} + 2\epsilon_b} \right) \left(\frac{\epsilon_a + 2\epsilon_b}{\epsilon_a - \epsilon_b} \right), \quad (2)$$

Bruggeman (Br) approximation

$$f_a = \frac{\left(\frac{\epsilon_{\text{eff}} - \epsilon_b}{\epsilon_{\text{eff}} + 2\epsilon_b} \right) \left(\frac{2}{3}\epsilon_{\text{eff}} + \frac{1}{3}\epsilon_a \right)}{\epsilon_{\text{eff}}(\epsilon_a - \epsilon_b)}. \quad (3)$$

Table 1. Volume fractions of iron oxide nanoparticles in a nanocomposite film calculated using the Maxwell–Garnett (MG) and Bruggeman (Br) approximations and the nanocomposite film thicknesses determined by ellipsometry and atomic force microscopy

Film structure	<i>f</i> of magnetite (MG)	<i>f</i> of magnetite (Br)	δ , nm (AFM)	δ , nm (ellipsometry)
PEI/(Fe ₃ O ₄ /PAH) ₆	0.13	0.12	58 ± 2	50 ± 3
PEI/(Fe ₃ O ₄ /PAH) ₁₁	0.25	0.24	84 ± 8	73 ± 1
PEI/(Fe ₃ O ₄ /PAH) ₁₆	0.55	0.53	111 ± 5	103 ± 2

The calculated volume fractions of magnetite nanoparticles in nanocomposite films are listed in Table 1. An analysis of the volume fractions of iron oxide nanoparticles calculated in terms of the Maxwell–Garnett and Bruggeman approximations suggests that the refractive index of the nanocomposite coating increases with the volume fraction of magnetite nanoparticles. This behavior was observed experimentally. The experimental data also agree well with the results in [19].

The SIMS results of studying nanocomposite films also support the increase in the volume fraction of magnetite nanoparticles in nanocomposite coatings.

The inset in Fig. 4 shows the mass spectra of an open substrate and the substrate coated with a film containing iron oxide nanoparticles. The curve of the coated substrate contains pronounced iron mass peaks (54, 56, 57u), which are absent in the case of the uncoated substrate. This fact confirms the transfer of magnetite nanoparticles to a single-crystal silicon wafer during polyionic assembly adsorption. Figure 4 also shows the SIMS concentration profiles of the nanocomposite films. The ion-beam speed was maintained at the same level. The time it takes for a

PEI/(Fe₃O₄/PAH)₆ nanocomposite film to be etched through (the beginning of the decrease in the curves in Fig. 4) is substantially shorter than the etching time of a PEI/(Fe₃O₄/PAH)₁₁ film. The time it takes for a PEI/(Fe₃O₄/PAH)₁₆ coating to be etched through is comparable with the etching time of a PEI/(Fe₃O₄/PAH)₁ film. Since the number of iron atoms in a film is proportional to the number of adsorbed layers, these results demonstrate that the iron atom concentration in the PEI/(Fe₃O₄/PAH)₁₆ film is highest. In turn, this finding corroborates the assumption that the volume fraction of magnetite nanoparticles increases in the films.

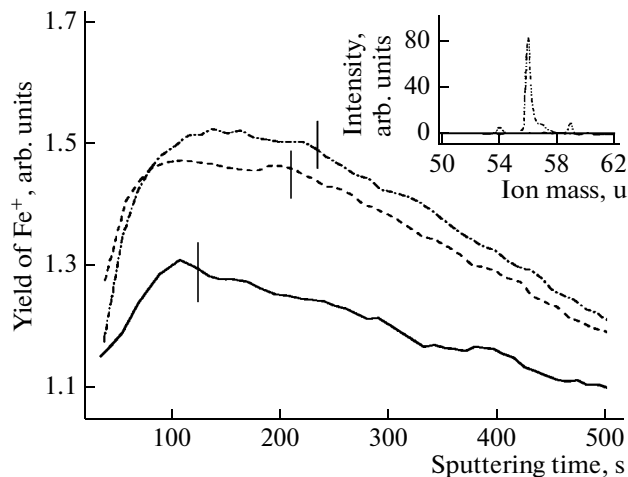


Fig. 4. Yield of secondary iron ions vs. the time of action of an ion beam on nanocomposite films (solid line) PEI/(Fe₃O₄/PAH)₆, (dashed line) PEI/(Fe₃O₄/PAH)₁₁, and (dot-and-dash line) PEI/(Fe₃O₄/PAH)₁₆. The vertical lines in the curves indicate the time it takes for the film to be etched through.

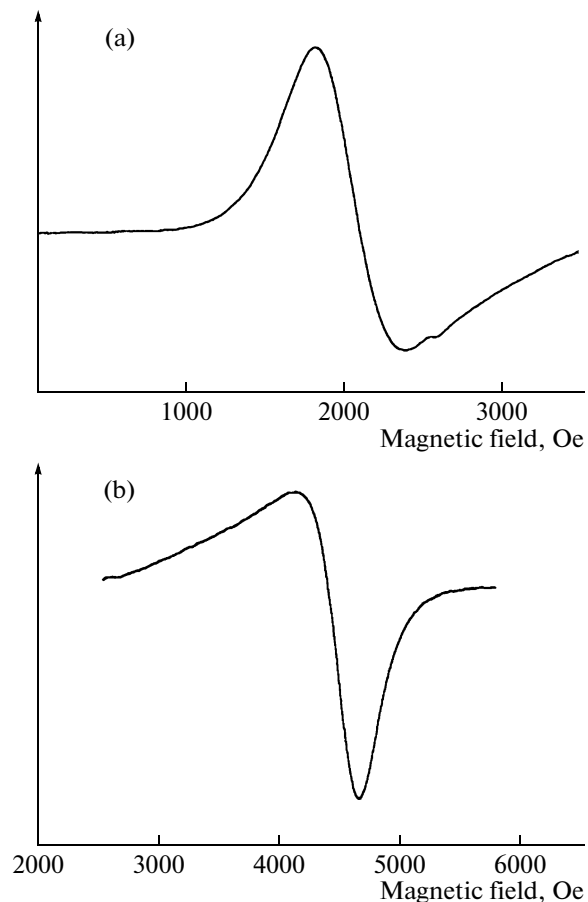


Fig. 5. EMR spectra of a PEI/(Fe₃O₄/PAH)₁₆ film for applied magnetic field H_0 oriented (a) parallel and (b) normal to the film plane.

Table 2. EMR characteristics for samples of two orientations

Film structure	I_{\perp} , arb.units	I_{\parallel} , arb.units	$\Delta H_{pp\perp}$, Oe	$\Delta H_{pp\parallel}$, Oe
PEI/(Fe ₃ O ₄ /PAH) ₆	155	60	710 ± 10	660 ± 10
PEI/(Fe ₃ O ₄ /PAH) ₁₁	385	590	560 ± 10	570 ± 10
PEI/(Fe ₃ O ₄ /PAH) ₁₆	1345	2350	510 ± 10	570 ± 10

Note: \perp (\parallel) indicates that an applied magnetic field is normal (parallel) to the film plane. I is the microwave absorption intensity (per unit area in the film), and ΔH_{pp} is the EMR line width.

The further decrease in the concentration profile in the films is caused by the crater effect [30].

A nonlinear character of the dependence of the properties of the films on the number of Fe₃O₄/PAH layers N in them is also supported by the EMR results. The EMR spectra (Fig. 5) of all films ($N = 6, 11, 16$) contain an intense broad line ($\Delta H_{pp} = 500–700$ Oe), and effective spectroscopic splitting factor g_{eff} depends on the film plane orientation with respect to applied magnetic field H_0 . To calculate the effective g factor, we used the formula

$$g_{\text{eff}} = 2.0023(H_e/H_R), \quad (4)$$

where H_R is the effective resonance field calculated by the peak-to-peak method and H_e is the resonance field corresponding to the g factor of a free electron. When the film plane is rotated from a position normal to an applied magnetic field to a position parallel to it, g_{eff} changes from 1.4 to 2.7.

Table 2 presents the values of line width ΔH_{pp} and magnetic resonance signal intensity I . It is interesting that, as the number of magnetic layers increases, the resonance signal does not broaden or even narrows,

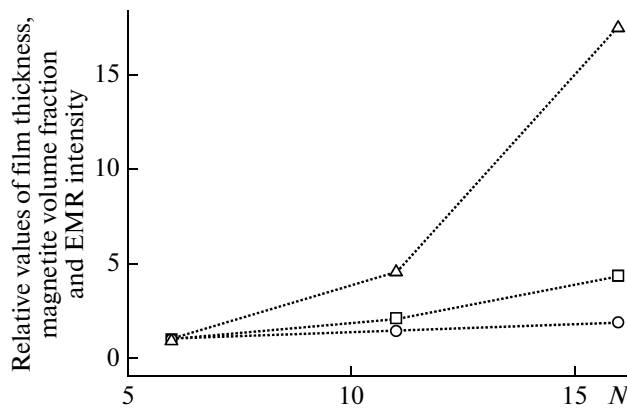


Fig. 6. Characteristics of the films vs. the number of Fe₃O₄/PAH layers N : (circles) film thickness (Table 1, AFM), (squares) magnetite content (Table 1, Br approximation), and (triangles) EMR signal intensity (the sum of the first two columns in Table 2). All values are normalized by the corresponding values at $N = 6$.

which can be due to an increase in the magnetic homogeneity of the samples.

The significant anisotropy in the effective g factor of the resonance line in nanocomposite films with iron oxide nanoparticles indicates a substantial magnetization in them. To estimate the magnetization of the samples, we use the following Kittel formula for a ferromagnetic resonance signal from a magnetic disk with allowance for the demagnetizing factor [31]:

$$\omega_0/|\gamma| = (H_{R,\parallel}(H_{R,\parallel} + 4\pi M))^{1/2}, \quad (5)$$

$$\omega_0/|\gamma| = H_{R,\perp} - 4\pi M. \quad (6)$$

Here, $\omega_0/|\gamma|$ is the resonance field for a ball sample; for bulk magnetite, it corresponds to $g_{\text{eff}} = 2.12$.

The magnetizations of the samples (150 kA/m) calculated by Eqs. (5) and (6) are approximately three times lower than that of the bulk phase of crystalline magnetite (480 kA/m).

The EMR line width and shape are almost independent of N . However, the EMR line intensity increases substantially with the number of magnetic layers (Fig. 6). For comparison, Fig. 6 also shows the relative change in the film thickness and the magnetite content in films. As is seen from Fig. 6, the nonlinear increase in the EMR signal intensity is caused by an increase in the density of the magnetic part of the films. As N increases, the magnetic layers become denser, which is likely due to an increase in their roughness. Since the EMR parameters (line width, effective g factor) change only weakly under these conditions, nanoparticles do not agglomerate and only the average interparticle distance decreases.

CONCLUSIONS

We prepared polyelectrolyte/iron oxide nanoparticles magnetic nanocomposite films on single-crystal silicon wafers. As the number of layers increases, the refractive index and roughness of the nanocomposite films increase. We studied the polyelectrolyte/magnetite nanoparticles multilayer structures by secondary-ion mass spectrometry and found that the increase in the refractive index and roughness of the films is related to an increase in the volume fraction of iron oxide nanoparticles. The volume fraction of iron oxide nanoparticles in a nanocomposite film is estimated using an effective medium model.

With electron magnetic resonance, we detected a significant anisotropy in the effective factor of the spectroscopic splitting of a resonance line and a noticeable nonlinearity in the dependence of the microwave absorption intensity on the number of magnetic nanoparticle layers in a film.

These results indicate that the optical and magnetic properties of the nanocomposite coatings can be controlled by varying the number of magnetic nanoparticle layers in them.

ACKNOWLEDGMENTS

This work was supported by the Russian Foundation for Basic Research (project nos. 06-02-04009, 08-03-01081) and the German DFG Foundation (project no. 436 RUS 113/844/0-1).

REFERENCES

1. M. C. Petty, *Langmuir-Blodgett Films: An Introduction* (Cambridge Univ., Cambridge, 1996).
2. G. B. Khomutov, *Adv. Colloid Interface Sci.* **111**, 79 (2004).
3. M. An and J.-D. Hing, *Thin Solid Films* **500**, 74 (2006).
4. J. B. Schlehoff, S. T. Dubas, and T. Farhat, *Langmuir* **16**, 9968 (2000).
5. M. Michel, A. Izquierdo, G. Decher, J.-C. Voegel, P. Schaaf, and V. Ball, *Langmuir* **21**, 7854 (2005).
6. G. Decher, *Science* **277**, 1232 (1997).
7. M. A. Correa-Duarte, M. Giersig, N. A. Kotov, and L. M. Liz-Marzan, *Langmuir* **14**, 6430 (1998).
8. J. Ruths, F. Essler, G. Decher, and H. Riegler, *Langmuir* **16**, 8871 (2000).
9. A. A. Mamedov and N. A. Kotov, *Langmuir* **16**, 5530 (2000).
10. A. Mamedov, J. Ostrander, F. Aliev, and N. A. Kotov, *Langmuir* **16**, 3941 (2000).
11. S. C. Tjong and G. D. Liang, *Mater. Chem. Phys.* **100**, 1 (2006).
12. S. P. Gubin, Yu. A. Koksharov, G. B. Khomutov, and G. Yu. Yurkov, *Usp. Khim.* **74**, 539 (2005).
13. N. M. Ushakov, I. D. Kosobudskii, G. Yu. Yurkov, S. P. Gubin, K. V. Zapsis, V. I. Kochubei, and A. N. Ul'zutuev, *Radiotekhnika* **10**, 105 (2005).
14. A. E. Varfolomeev, A. V. Volkov, D. Yu. Godovskii, G. A. Kapustin, and M. A. Moskvina, *Pis'ma Zh. Eksp. Teor. Fiz.* **67**, 37 (1998) [*JETP Lett.* **67**, 39 (1998)].
15. K. A. Zvezdin, *Fiz. Tverd. Tela* (St. Petersburg) **42**, 116 (2000) [*Phys. Solid State* **42**, 120 (2000)].
16. S.-S. Kim, S.-T. Kim, J.-M. Ahn, and K.-H. Kim, *J. Magn. Magn. Mater.* **271**, 39 (2004).
17. S. W. Kingman and N. A. Rowson, *Mineral Eng.* **11**, 1081 (1998).
18. S. A. Portnov, A. M. Yashchenok, A. S. Gubskii, D. A. Gorin, A. A. Neveshkin, B. N. Klimov, A. A. Nefedov, and M. V. Lomova, *Prib. Tekh. Eksp.* **5**, 1 (2006).
19. D. Grigoriev, D. Gorin, G. B. Sukhorukov, A. Yashchenok, E. Mal'tseva, and H. Möhwald, *Langmuir* **23**, 12388 (2007).
20. D. G. Shchukin, G. B. Sukhorukov, and H. Möhwald, *Angew. Chem. Int. Ed. Engl.* **42**, 4472 (2003).
21. N. Gaponik, I. L. Radthenko, G. B. Sukhorukov, and A. L. Rogach, *Langmuir* **20**, 1449 (2004).
22. S. Köstler, A. V. Delgado, and V. Ribitsch, *J. Colloid Interface Sci.* **286**, 339 (2005).
23. M. Kolasinska and P. Warszynski, *Appl. Surf. Sci.* **252**, 759 (2005).
24. M. Kolasinska, R. Krastev, and P. Warszynski, *J. Colloid Interface Sci.* **305**, 46 (2007).
25. D. I. Bilenko, V. P. Polyanskaya, M. A. Gets'man, D. A. Gorin, A. A. Neveshkin, and A. M. Yashchenok, *Zh. Tekh. Fiz.* **75** (6), 69 (2005) [*Tech. Phys.* **50**, 742 (2005)].
26. A. G. Rokakh, A. G. Zhukov, S. V. Stetsura, and A. A. Serdobintsev, *Nucl. Instrum. Methods Phys. Res. B* **226**, 595 (2004).
27. J. J. Harris and M. L. Bruening, *Langmuir* **16**, 2006 (2000).
28. A. Neff, A. Naji, C. Ecker, B. Nickel, R. Klitzing, and A. R. Bausch, *Macromolecules* **39**, 443 (2006).
29. N. Nagy, A. Deak, Z. Horvolgyi, M. Fried, A. Agod, and I. Barsony, *Langmuir* **22**, 8416 (2006).
30. L. Feldman and D. Mayer, *Fundamentals of Surface and Thin Film Analysis* (North-Holland, New York, 1986; Mir, Moscow, 1989).
31. C. Kittel, *Introduction to Solid State Physics* (Wiley, New York, 1976; Nauka, Moscow, 1978).

Translated by K. Shakhevich